Tectonophysics 493 (2010) 254–262

Contents lists available at ScienceDirect

Tectonophysics

journal homepage: www.elsevier.com/locate/tecto

The effect of asymmetric damage on dynamic shear rupture propagation I: No mismatch in bulk elasticity

R.L. Biegel [a], H.S. Bhat [a,b,*], C.G. Sammis [a], A.J. Rosakis [b]

[a] Department of Earth Sciences, 3651 Trousdale Parkway, Los Angeles, CA 90089, USA
[b] Graduate Aerospace Laboratories, 1200 East California Boulevard, Pasadena, CA 91125, USA

ARTICLE INFO

Article history:
Received 1 October 2009
Received in revised form 27 February 2010
Accepted 24 March 2010
Available online 28 March 2010

Keywords:
Dynamic shear rupture
Bimaterial ruptures
Damage mechanics
Supershear

ABSTRACT

High-speed digital photography was used to study rupture propagation on the interface between transparent damaged and undamaged photoelastic plates. Bilateral ruptures were nucleated on pre-machined faults at an angle α to the uniaxial loading axis. Stress concentration at the crack tips produced fringes in polarized laser light that allowed their positions to be measured in successive photos. We found that fracture damage introduces a strong asymmetry in propagation speed different from that expected due to the lower elastic stiffness in the damaged material alone. When the tensile lobe of a rupture tip propagated through the damaged material the velocity of that rupture was reduced or stopped. By contrast, when the compressive lobe of a rupture tip passed through the damage, the velocity of that rupture was unaffected by the damage. A physical interpretation is that passage of a tensile lobe through the damage expends energy by lowering the normal stress on pre-existing cracks thus allowing frictional sliding along the crack surfaces. When the compressive lobe of the rupture passes through the damage, compressive stresses prevent sliding, only minor energy is dissipated, and the damage has almost no effect on the velocity. This effect can produce asymmetric propagation for earthquake ruptures on slip surfaces near the edge of a highly damaged fault zone.

1. Introduction

Large displacement faults often juxtapose rocks with different elastic stiffness across the fault plane. Experimental and theoretical studies on such elastic bimaterial interfaces have found that propagation is asymmetric ((Rosakis et al., 2007) and references therein). A rupture propagating in the direction of motion of the more compliant material (the material with lower elastic wave speeds, commonly termed the positive '+' direction) travels with a different speed than a rupture propagating in the opposite negative '−' direction. Numerical studies have shown that this asymmetric propagation is caused by a reduction in the normal stress at the tip of ruptures propagating in the '+' direction, thus making the rupture asymmetric (Weertman, 1980; Andrews and Ben-Zion, 1997; Harris and Day, 1997; Cochard and Rice, 2000; Rice, 2001; Ranjith and Rice, 2001; Ben-Zion, 2001; Xia et al., 2005b; Shi and Ben-Zion, 2006; Rubin and Ampuero, 2007).

Experimental studies of rupture propagation on bimaterial interfaces by (Xia et al., 2005b) observed bilateral asymmetric propagation in all cases. Ruptures in the '+' direction propagated at the generalized Rayleigh wave speed while those in the '−' direction transitioned to supershear speeds approaching P_{slow}, the P wave speed in the slower (more compliant) material.

These results are consistent with the seismological observation of asymmetric supershear propagation in the '−' direction during the 1999 Izmit earthquake on the North Anatolian Fault in Turkey (Bouchon et al., 2001; Rosakis et al., 2007) and with numerical simulations (Harris and Day, 1997,2005.

Field studies suggest that this representation of a fault as a planar contact between two intact elastic wall rocks may be too simple. In real faults, many of which have been exhumed from seismogenic depths by uplift and erosion, the wall rocks are separated by layers of fragmented rock classified according to grain size as fault breccia, gouge, or cataclasite as in Fig. 1 (see (Ben-Zion and Sammis, 2003), (Biegel and Sammis, 2004), (Bizzarri, 2009) and references therein for a more complete review of fault zone structure). For the San Andreas fault, a 100–200 m wide low velocity zone associated with this fragmented layer has been mapped seismically to depths of 7 km (Li and Malin, 2008). Seismic velocities have been observed to decrease in the fragmented layer during an earthquake followed by an exponential-like recovery over time suggesting an interaction between the propagating rupture and the fracture damage (Marone et al., 1995; Li and Vidale, 2001; Li et al., 2003).

Theoretical and experimental studies have demonstrated that off-fault damage can reduce rupture speed below that due to the decrease in elastic stiffness alone (Andrews, 2005; Templeton and Rice, 2007;

* Corresponding author. Department of Earth Sciences, 3651 Trousdale Parkway, Los Angeles, CA 90089, USA.
E-mail address: hbhat@usc.edu (H.S. Bhat).

0040-1951/$ – see front matter © 2010 Elsevier B.V. All rights reserved.
doi:10.1016/j.tecto.2010.03.020

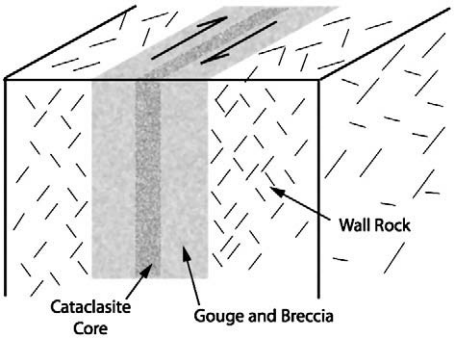

Fig. 1. Schematic diagram of a fault zone. Most of the slip is accommodated in the fault core, which is typically a few cm thick and is composed of very fine grained crushed rock called cataclasite. Slip is usually further localized on very narrow slip surfaces within the core. The core is bordered by layers of coarser fragmented rock called gouge or breccia. These layers are usually a few meters thick and appear to be shattered in place with little or no shear strain. The gouge and breccia is bordered by fractured by not granulated wall rock in which the fracture density decreases with distance from the fault zone, falling to the background density over a distance of a few hundred meters. More detail is given in reviews by (Ben-Zion and Sammis, 2003) and (Biegel and Sammis, 2004) and references therein.

Biegel et al., 2008). In these studies, the additional slowing appears to be caused by non-linear dissipation in the stress concentrations at the crack tip. (Rice et al., 2005) have shown that the spatial extent of the interaction between the tip of a propagating slip pulse and off-fault damage is approximately the same as the distance behind the crack tip over which friction decreases from its static to its lower dynamic value, commonly termed R_0. By fitting the slip distributions measured by (Heaton, 1990) for seven large earthquakes, they found that R_0 ranged from meters to ten of meters at the centroid depths of the earthquakes (typically between 5 and 15 km). In contrast R_o for Homalite, the photoelastic polymer we use in the experiments presented here, has been calculated and measured by (Biegel et al., 2008) to be about 1 cm for our loading conditions. The critical stress intensity factor, K_{IC}, and frictional behavior of Homalite are known, and are comparable to those of rock. The primary differences between Homalite and rock are the lower elastic moduli in the polymer. This reduced stiffness produces the smaller value of R_0 and a comparably small nucleation patch size which allows dynamic ruptures to be studied at laboratory length scales (see (Xia et al., 2004)). Scaling between Homalite and rock has been discussed in detail by (Biegel et al., 2008).

The question we wish to address here is whether the fault zone damaged layer can produce additional asymmetric propagation beyond that caused by a contrast in undamaged wall rock stiffness across the fault plane. If the earthquake rupture propagates on a localized surface down the center of the damaged layer, then symmetry precludes this scenario. However, if slip is localized at or near the boundary between a damaged layer and the wall rock, then it is possible that the lower velocity in the damaged layer, or anelastic dissipation in the fragmented rock, or both may produce additional asymmetry in the propagation. The demonstration by (Rice et al., 2005) that the spatial scale of interaction is the same order as the spatial extent of the damaged layer suggests that such asymmetry may be possible.

In this paper we use high-speed digital photography to study the propagation of ruptures on the interface between damaged and undamaged photoelastic Homalite plates in the laboratory. We find that fracture damage introduces a strong propagation asymmetry beyond that expected due to the lower elastic stiffness in the damaged material.

2. Experimental apparatus and procedures

We use the same apparatus and follow the same procedures described by (Xia et al., 2004), (Xia et al., 2005b), (Rosakis et al., 2007), (Lu et al., 2007) and (Biegel et al., 2008). Square plates of the transparent photoelastic polymer Homalite (15.25 cm × 15.25 cm × 1 cm) were bisected by a saw-cut fault at an angle α to one edge. The contacting faces were lapped with #220 sandpaper. Mean surface roughness was measured to be about 2 mm using a digital contact profilometer. As shown in Fig. 2, the samples were loaded with uniaxial stress P and a dynamic fracture was nucleated by using a high voltage pulse to explode a wire across the center of the fault plane. The explosion reduced normal stress on a patch of the fault approximately 1 cm long thereby nucleating a rupture which, in most cases, propagated bilaterally. The voltage pulse also triggered high-speed digital cameras which take a series of pictures of the propagating rupture using transmitted polarized light that resolved the photoelastic fringes produced by the spatial gradients in shear stress (Fig. 3). The experiments described here differ from those in previous studies in that the half-plate below the fault was fracture damaged as shown in Fig. 3. Fracture damage was generated as described in (Biegel et al., 2008) by using a razor knife to produce a grid of scratches approximately 2 mm apart (chosen simply for convenience rather than mimicking real earth damage density) oriented at ±45° to the loading axis, and then dipping the plate in liquid nitrogen for about 45 s.

3. Elastic properties of damaged Homalite

The elastic properties of undamaged and damaged Homalite are summarized in Table 1. The shear speed in damaged Homalite was measured in the dynamic rupture experiments by (Biegel et al., 2008). The observed decrease in shear speed corresponds to a fracture density parameter near $=0.2$ in the (O'Connell and Budiansky, 1974) model. For this value of , their model predicts a 20% reduction in P wave speed c_p^d (where the superscript d stands for 'damage') and a 17% reduction in Poisson's ratio ν, as in Table 1.

The value of $=0.2$ was calculated from the observed reduction in c_s is consistent with the value calculated using its definition $=N_V\langle a^3\rangle$ in terms of the observed volume density $N_V=1.1$ m cm^3 and average radius $a=0.6$ cm of the fractures found using standard stereology (see (Biegel et al., 2008)).

An important parameter used to describe mode II rupture propagation on the interface between two elastic materials with different moduli is the generalized Rayleigh speed which is found by solving the following equation (Rice, 2001):

$$f(V) = \left(1-b_1^2\right)a_1G_2D_2 + \left(1-b_2^2\right)a_2G_1D_1 = 0 \quad (1)$$

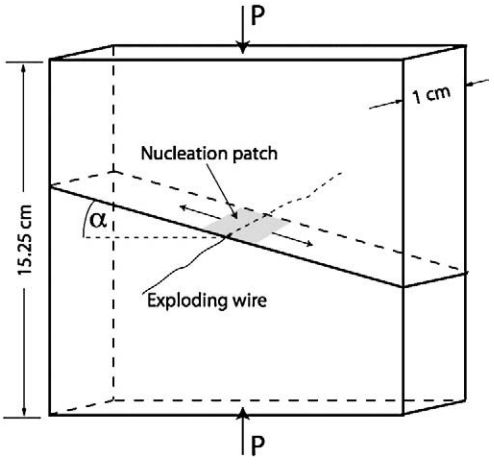

Fig. 2. Sample geometry. Homalite plate bisected by a pre-machined fault at an angle α is loaded in uniaxial compression P. Exploding wire reduces normal stress on a fault patch which nucleates a bilateral rupture. For details see (Rosakis et al., 2007).

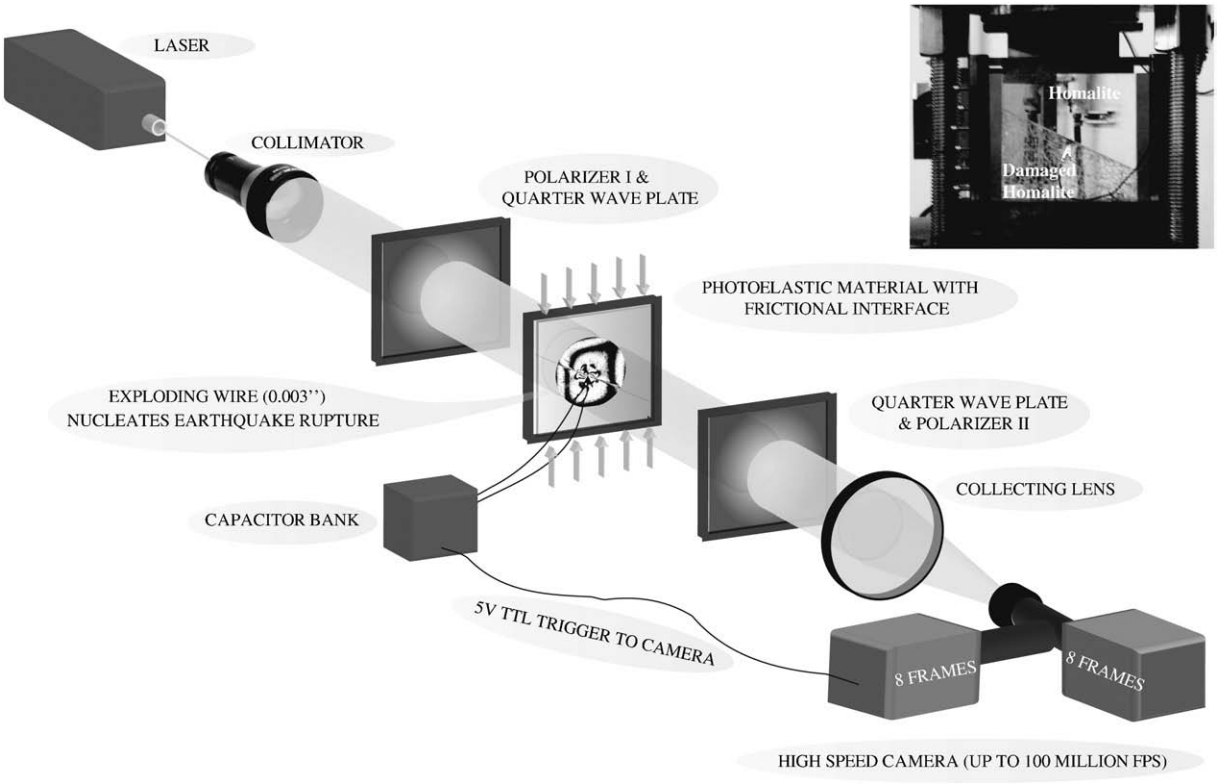

Fig. 3. Experimental apparatus used to photograph shear stress fringes in a Homalite sample during dynamic rupture. Inset shows sample in loading frame used to apply uniaxial load P. The saw-cut fault separating damaged and undamaged Homalite has a normal vector at an angle α to the load. For details see (Rosakis et al., 2007).

where $a_n = \sqrt{1-\left(V/c_p^n\right)^2}$, $b_n = \sqrt{1-\left(V/c_s^n\right)^2}$ and $D_n = 4a_nb_n - (1-b_n^2)^2$. In these expressions, V is the rupture speed, G_n are the rigidity of the two materials ($n=1, 2$), c_s^n and c_p^n are the S and the P wave speeds respectively of the two materials ($n=1, 2$). Using the elastic properties in Table 1, this equation gives $c_{GR}=996$ m/s for an interface between damaged and undamaged Homalite.

4. Measurement of rupture velocity and supershear transition length

We measured the crack tip position as a function of time from the isochromatic fringe patterns in successive high-speed digital images. These data were then fit with either an interpolating cubic spline or a smoothing spline using the curve fitting toolbox in MATLAB®. The resulting fit was then differentiated to obtain instantaneous rupture velocity as a function of time. Rupture velocities in the supershear regime were checked by measuring the Mach angle, β, in the photographs and using the relationship $v_r/c_s = 1/\sin\beta$ where v_r is the rupture velocity.

Once rupture velocity was determined as a function of time, the data were interpolated to obtain the exact time at which the rupture speed reached c_s, the shear wave speed in Homalite. This time was then used to obtain the corresponding distance at which the supershear transition took place by interpolating the rupture position as a function of time. The transition length was determined for both the left and right crack tips, L_T^l and L_T^r respectively. This analysis was done for velocities obtained using both spline fits. Where they differed, the one that gave an interpolated transition length that was most consistent with the first appearance of a Mach cone in the photos was chosen. In cases where the rupture had already transitioned to supershear speed by the time the first photograph was taken, we estimated the transition length using the geometrical relationship given by (Rosakis et al., 2007) (see Section 4.06.3.2 of that paper).

Table 1
Material properties of sample materials.

	c_p (m/s)	c_s (m/s)	ν	ε
Homalite	2498[a]	1200[a]	0.35[a]	0
Damaged Homalite	2000[c]	1000[b]	0.25[c]	0.2

[a] Rosakis et al. (2007).
[b] Biegel et al. (2008).
[c] O'Connell and Budiansky (1974).

5. Dynamic shear rupture propagation on a Homalite/Homalite interface

We begin with rupture experiments in undamaged Homalite for comparison with (Xia et al., 2004) and for comparison with ruptures on the interface between damage and undamaged Homalite presented in a later section. Two cases are reported here, one at $P=12$ MPa and one at $P=15$ MPa (both had a fault angle of $\alpha=25°$). Results of the 12 MPa case are summarized in Fig. 4.

Our observations agree with (Xia et al., 2004, 2005a) in that propagation is almost symmetric and both rupture tips transition to supershear speeds. The slight asymmetry in propagation may be due to a corresponding spatial asymmetry in surface roughness of the interface. However our transition lengths are significantly different than those measured by (Xia et al., 2004, 2005a), which may reflect a difference in either surface preparation or nucleation strength (Lu et al., 2008). Nevertheless, as discussed by (Rosakis et al., 2007), our transition lengths decrease with increasing load.

In both cases the rupture accelerates toward the P wave speed of Homalite. The oscillations in rupture velocity may reflect the accuracy to which we can pick the position of the crack tip in the photos. An uncertainty in position of 0.5 mm leads to an uncertainty of about 200 m/s in instantaneous velocity. Oscillations might also be caused by subtle variations in surface roughness along the interface.

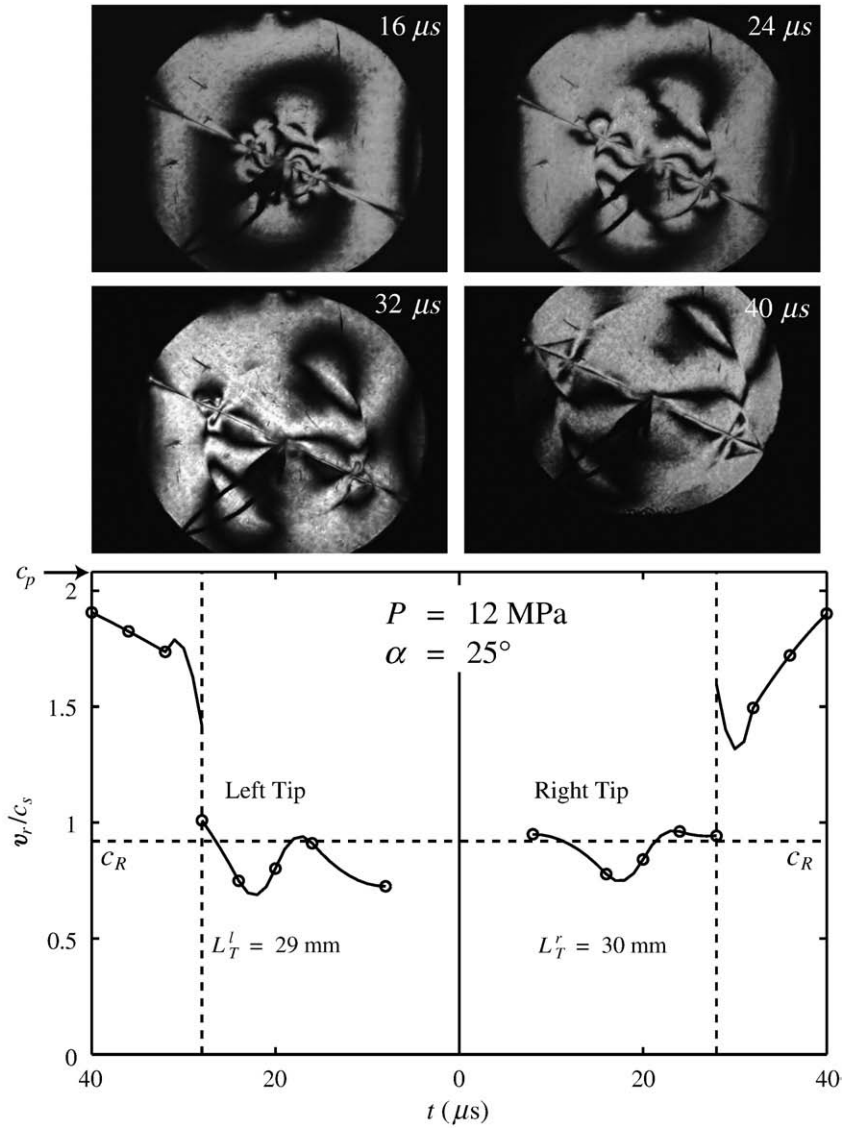

Fig. 4. Snapshots of isochromatic fringe pattern showing contours of maximum shear stress due to a dynamic shear rupture along a frictional interface between two undamaged Homalite plates for applied load, P = 12 MPa and fault angle, $\alpha = 25°$. The rupture undergoes a Burridge–Andrews (Burridge, 1973; Andrews, 1976) type supershear transition at $t = 28$ μs. Normalized rupture velocity v_r/c_s is plotted as a function of time for the left and right crack tips. Open circles indicate times at which the pictures were taken and the solid curves are the instantaneous rupture velocity found by differentiating cubic spline fits to the measured crack tip positions as discussed in the text. Also shown are the normalized Rayleigh wave speed c_R/c_s and normalized P wave speed $c_p/c_s = 2.08$ (upper boundary of the graph). L_T^l and L_T^r are the measured (or extrapolated) supershear transition lengths for the left and right crack tips respectively.

For $P = 15$ MPa and $\alpha = 25°$, recent experiments by (Lu et al., 2007) show that a crack-like propagation mode is favored over a slip pulse. Crack-like propagation in our experiment is supported by a propagating front in the isochromatics, behind the main supershear rupture front, that propagates at the Rayleigh wave speed.

6. Dynamic shear rupture on the interface between Homalite and damaged Homalite

To explore rupture directionality produced by asymmetric off-fault damage, we conducted a series of experiments in which ruptures propagated on the interface between damaged and undamaged Homalite. As illustrated in Fig. 5, dynamic symmetry in these experiments is broken in two different ways. First, the contrast in 'static' elastic stiffness between damaged and undamaged Homalite introduces the elastic asymmetry described by the '+' and '−' propagation directions as previously discussed by (Xia et al., 2005b). Second, the stress concentration at the rupture tip introduces 'dynamic' anelastic asymmetry based on whether the tensile or compressive lobe of the crack tip stress concentration is on the damaged side of the interface. Here we introduce a new convention associated with rupture direction. The side or direction of the rupture that places the compressive stress lobe, associated with the rupture tip, on the damaged material is called the '*C*' side or direction. Similarly the '*T*' side or direction corresponds to the rupture tip associated tensile stress field being on the damaged side. When this is combined with the '+' and '−' directions associated with material mismatch we get the following relevant combinations of sides or directions.

i. '*C*+' and '*T*−' when a right-lateral rupture is bounded on top ($y>0$ domain) by an undamaged material of greater bulk elastic moduli which is discussed in this paper. [These asymmetries are illustrated in Fig. 5 which shows that ruptures propagating to the left are '*C*+' while those propagating to the right are '*T*−']
ii. '*C*−' and '*T*+' when a right-lateral rupture is bounded on bottom ($y<0$ domain) by an undamaged material of lower bulk elastic moduli which is discussed in part II of this paper (Bhat et al., 2010-this issue).

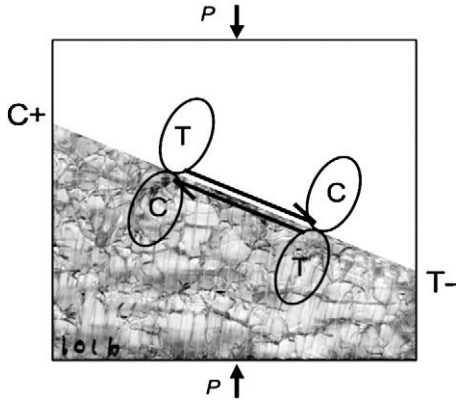

Fig. 5. Anelastic asymmetry results from the positions of the compressive and tensile stress concentration lobes of the two crack tips within the damaged Homalite. In the '*C*' direction, the compressive lobe is in the damage while in the '*T*' direction the tensile lobe is in the damage. Also shown are the '+' and '−' directions defined by the elastic contrast across the fault. The '+' direction is defined as the direction of motion of the more compliant wall rock (damaged Homalite in this case).

More anelastic loss is expected at the rupture tip that propagates in the direction for which its tensile lobe is on the damaged side of the interface, which we term the '*T*' direction. Less loss is expected in the opposite '*C*' direction which places the damaged side in compression. The asymmetry arises because local tension relives normal stress to enhance frictional sliding on the fractures comprising the damage and may even result in local mode I fracture growth. In contrast, local compression increases the normal load which suppressed sliding. This is a key feature of these experiments. In addition to the drop in the elastic moduli due to the presence of micro-cracks (say when measured using uniaxial tensile or compressive tests under quasi-static conditions) there is a dynamic response of the material associated with the rupture itself which changes the elastic moduli dynamically both spatially and temporally. The spatial heterogeneity comes from the anti-symmetric stress field associated with the rupture whereas the temporal heterogeneity arises from the dynamic stress field variation with time. Since less loss in elastic moduli is expected along the '*C*' direction the rupture propagates along an interface bounded by two media of almost same elastic moduli.

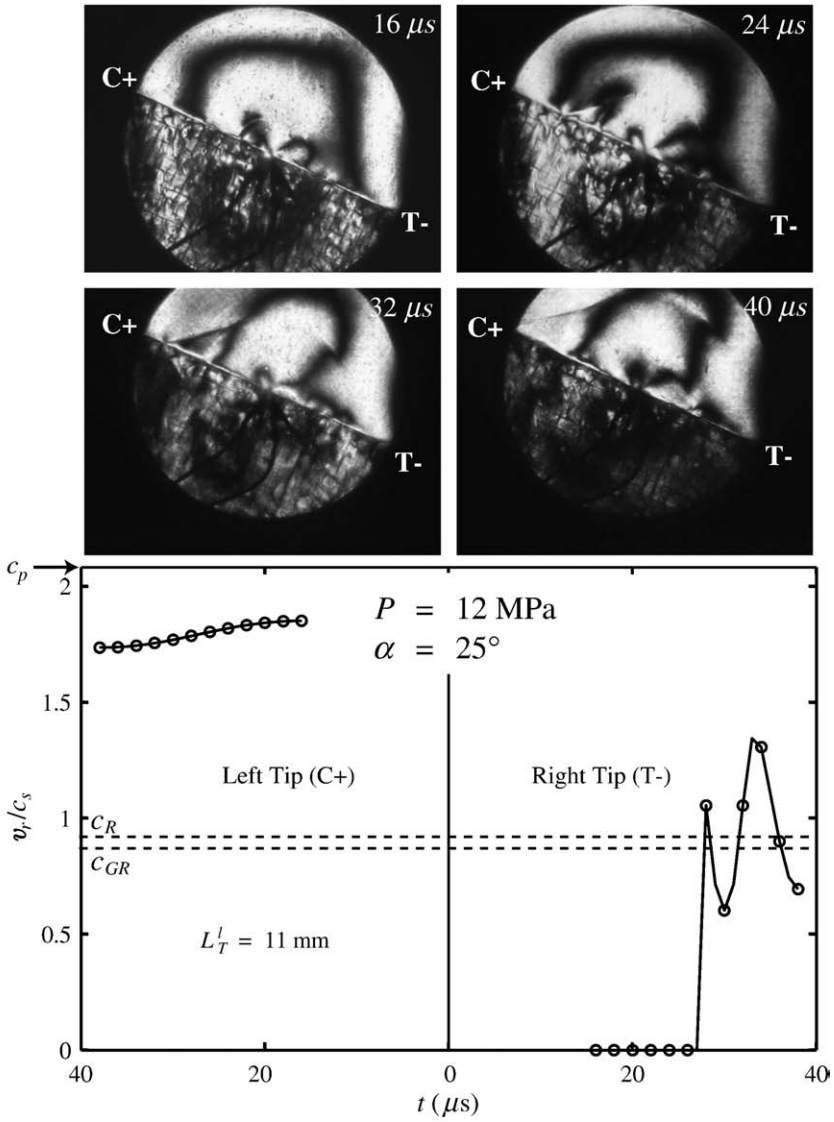

Fig. 6. Snapshots of isochromatic fringe pattern showing contours of maximum shear stress due to a dynamic shear rupture along a frictional interface separating Homalite and damaged Homalite for an applied load $P=12$ MPa and a fault angle $\alpha=25°$. Normalized rupture velocity v_r/c_s is plotted as a function of time for the left and right crack tips. Open circles indicate times at which the pictures were taken and the solid curves are the instantaneous rupture velocity found by differentiating cubic spline fits to the measured crack tip positions as discussed in the text. Also shown are the normalized generalized Rayleigh wave speed c_R/c_s and normalized P wave speed $c_p/c_s=2.08$ (upper boundary of the graph). L_T^l is the measured (or extrapolated) supershear transition length for the left crack tip. All velocities are normalized to c_s the shear wave speed in undamaged Homalite.

This falls under the category of homogeneous ruptures. When the bulk elastic properties of the damaged and the undamaged materials bounding the fault are different we expect a classical bimaterial rupture along the '*C*' direction. For the sake of clarity we first study the case of homogeneous ruptures in the '*C*' direction. The bimaterial ruptures in the '*C*' direction is discussed in part II of this paper by (Bhat et al., 2010-this issue).

Experiments with three different combinations of uniaxial load and fault angle are presented here: $P=12$ MPa and $\alpha=25°$, $P=15$ MPa and $\alpha=25°$, and $P=20$ MPa and $\alpha=28°$. Results for the case $P=12$ MPa and $\alpha=25°$ are given in Fig. 6 where it is obvious that rupture propagation is strongly asymmetric. The rupture propagating to the right (in the '*T*−' direction) is suppressed for about 26 μs before accelerating to a rupture speed that oscillates around the generalized Rayleigh wave speed c_{GR}. Rupture propagation to the left (in the '*C*+' direction) transitions to supershear speed almost immediately upon nucleation and accelerates toward the *P* wave speed in undamaged Homalite. This behavior is quite different from that observed by (Xia et al., 2004, 2005a) for ruptures on the interface between Homalite and polycarbonate where, for the same *P* and α, rupture in the '+' direction propagated at c_{GR} while rupture in the '−' direction propagated at the supershear speed P_{slow}, the *P* wave speed in the more compliant polycarbonate. Since the contrast in shear wave speed across the fault plane is comparable in both systems (80% for polycarbonate/Homalite and 83%for damaged Homalite/Homalite), the very different nature of the observed asymmetry implies that damage plays an important mechanical role beyond just reducing the wave speeds.

We propose the following explanation of these observations. Propagation at c_p in the $C+$ direction is the same behavior observed for undamaged Homalite in Fig. 4. We hypothesize that compression at the crack tip immobilizes the flaws comprising the damage and

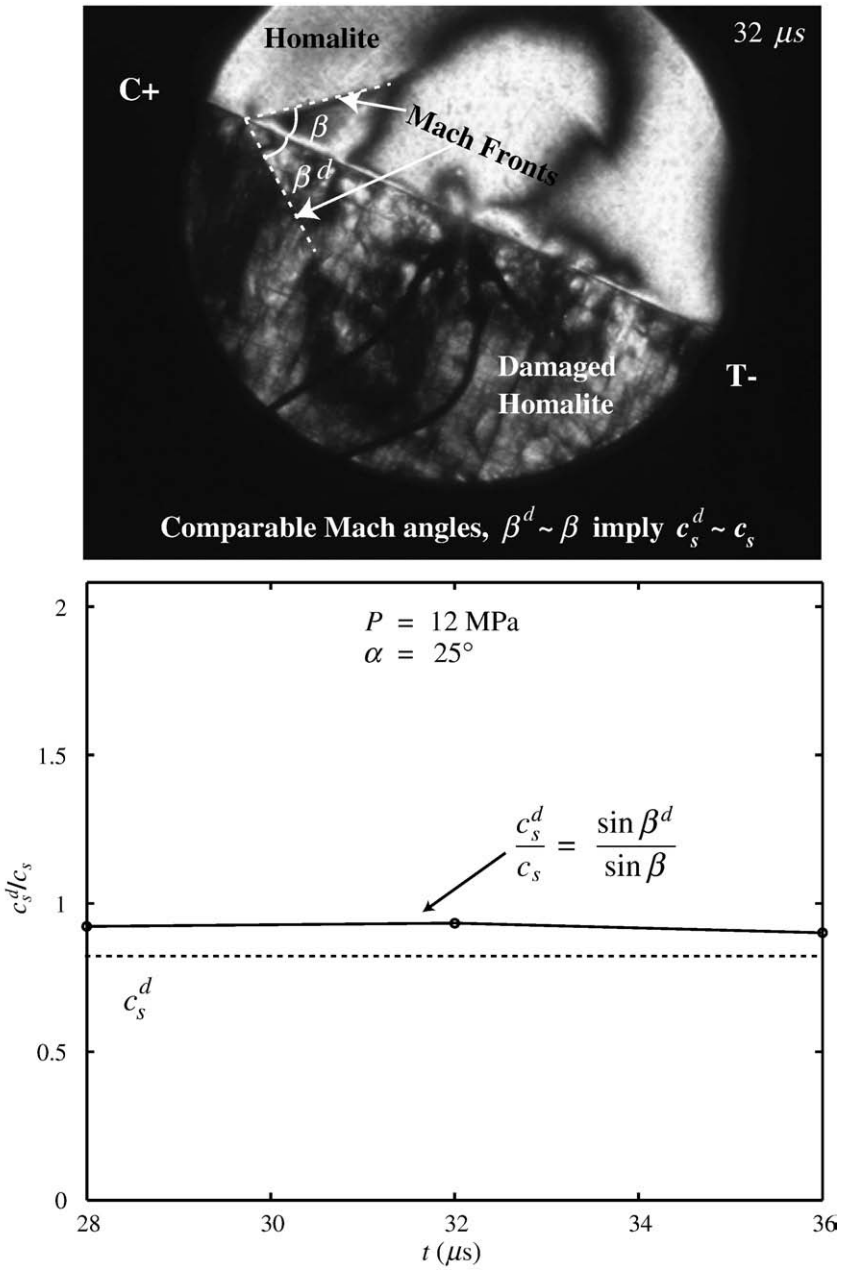

Fig. 7. Comparison of Mach angles β in Homalite and β^d in damaged Homalite. Upper panel shows the frame at 32 μs from Fig. 6. The lower panel shows the ratio of shear velocities in the damaged and undamaged Homalite. c_s^d is the expected value of the ratio for shear wave speeds in damaged and undamaged Homalite from Table 1. A complete deactivation of the damage by compression would give 1.0.

they play no role in dynamic propagation. This hypothesis is supported by the observation in Fig. 7 that the Mach angles in Homalite and damaged Homalite are nearly equal. The ratio between the *S*-wave speed in Homalite and in damaged Homalite is related the ratio of the Mach angles as

$$\frac{c_s^d}{c_s} = \frac{\sin\beta^d}{\sin\beta} \tag{2}$$

where the superscript '*d*' refers to damaged Homalite. This ratio is plotted as a function of time in Fig. 7. Based on the measured velocities in Table 1, the expected ratio is 0.83. The observed value is closer to 0.9 which supports our hypothesis that the mechanical effects of the damage are suppressed on the compressive side of the rupture.

We hypothesize that the delay in propagation in the '*T*−' direction is caused by a significant lowering of the effective elastic modulus on the damaged side of the interface due to activation of the damage by the tension and the activation of off-fault energy dissipation due to frictional sliding. This lower modulus reduces the stress intensity factor (which is a measure of the strength of the crack tip stress field) below its critical value for propagation. As the rupture length increases in the '*C*+' direction, the stress intensity factor at the '*T*−' tip increases as the square root of the length of the rupture until it reaches the critical value (a material property) and rupture is initiated (at about $t = 26\,\mu s$).

When the applied load is increased to 15 MPa at the same fault angle $\alpha = 25°$, the rupture on the '*C*+' side once again initiates and propagates at supershear speed whereas the rupture on the '*T*−' side now propagates slightly below the Rayleigh wave speed of Homalite (Fig. 8). The slight reduction in rupture velocity, compared to the previous case, may be due to increased damage activation at the higher applied load. Note that the rupture on the '*T*−' side was not delayed in this case.

In Fig. 9 the load was increased to $P = 20$ MPa and the fault angle to $\alpha = 28°$. In this case the rupture propagated unilaterally at a supershear speed near c_p in the '*C*+' direction. In order to understand this result, consider the case of uniaxial loading where the ratio of the resolved shear, τ, to the normal stress (positive in compression), σ, acting on the fault depends only on the fault angle and is given by

$$\frac{\tau}{\sigma} = \frac{\sin 2\alpha}{1 + \cos 2\alpha} \tag{3}$$

By increasing the fault angle from 25° to 28° we have increased τ/σ and brought the fault closer to failure (f_s, the static coefficient of friction, ≈ 0.6 for Homalite). By increasing the applied load from 15 to

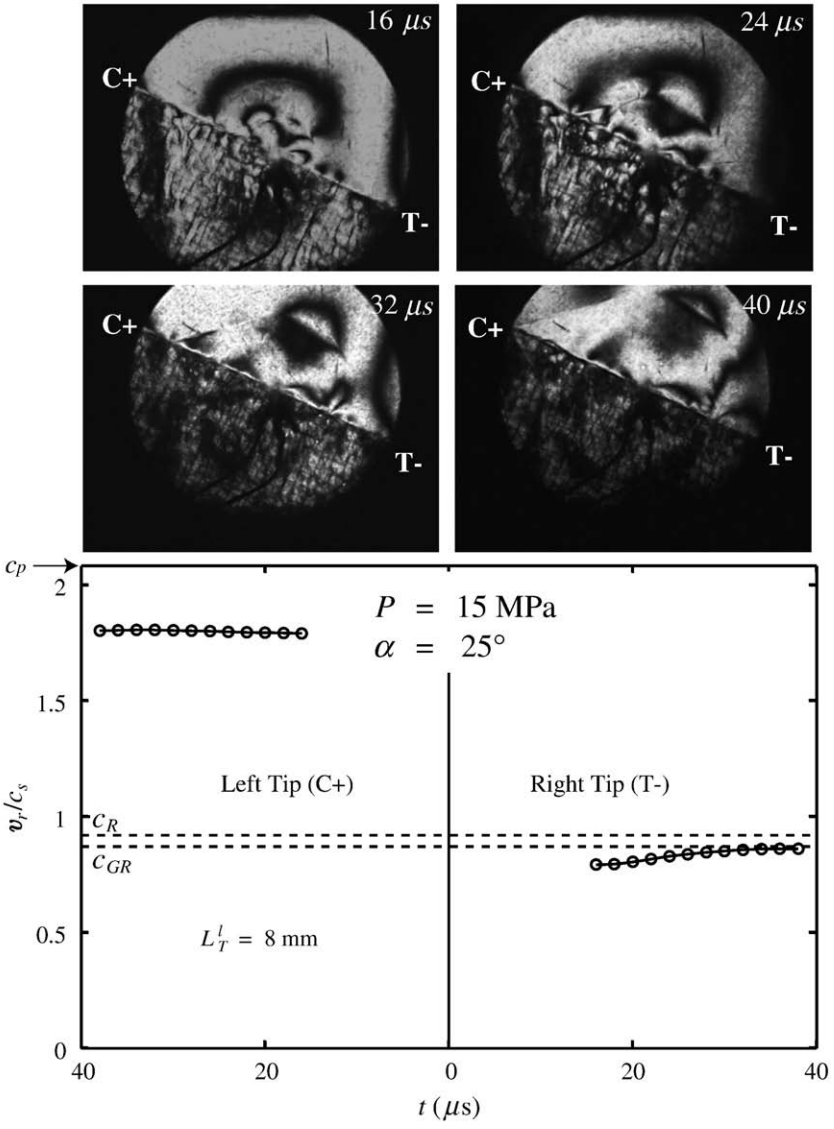

Fig. 8. Same as Fig. 6 except the applied load, $P = 15$ MPa.

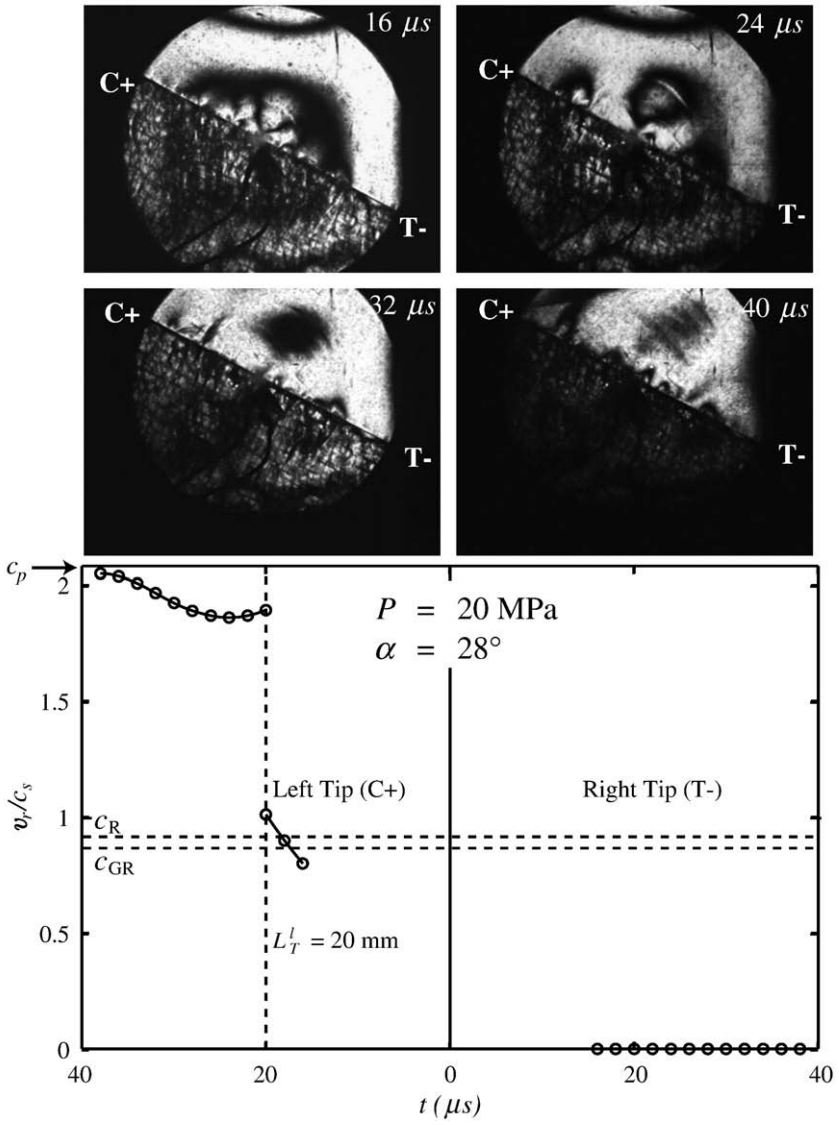

Fig. 9. Same as Fig. 6 except the applied load is $P=20$ MPa and the fault angle is $\alpha=28°$.

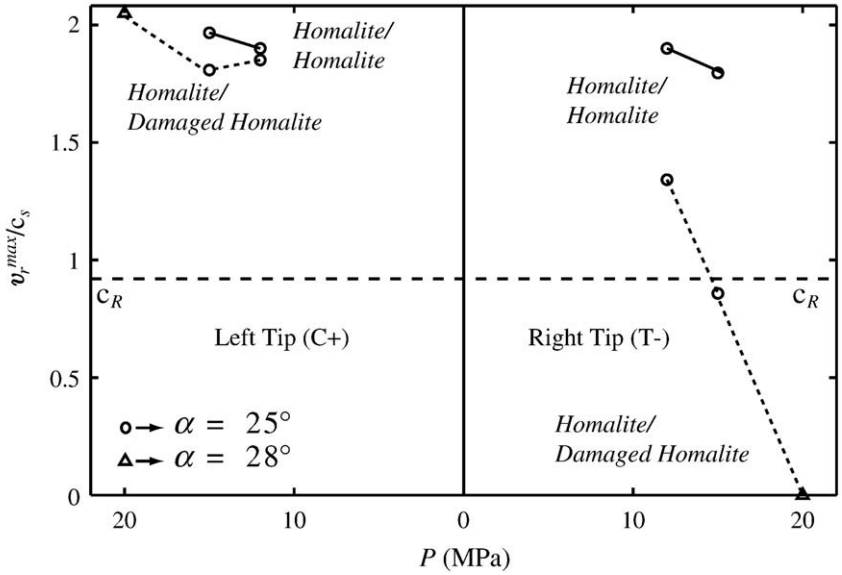

Fig. 10. The effect of load on maximum rupture velocity of a dynamic shear rupture on the interface between Homalite and damaged Homalite. Velocities are also shown at the same pressures for rupture on the interface between two undamaged Homalite plates for comparison. All velocities are scaled to c_s, the shear wave speed in undamaged Homalite.

20 MPa we have increased the off-fault stress levels thereby also increasing the effect of damage in retarding or stopping the rupture in the '$T-$' direction. Thus even though the resolved shear stress was increased on the fault, the increased damage activation completely suppressed rupture in the '$T-$' direction.

7. Summary and conclusions

We have studied the effect of off-fault damage on dynamic rupture propagation. When a fault separates an intact material from the same material which is fracture damaged, the rupture prefers to propagate in the direction for which the compressive stress lobe is in the damaged material. We denote this direction as '$C+$'. In the opposite direction for which the tensile stress lobe is in the damaged material, '$T-$', the rupture propagation is retarded or completely stopped due to two effects. First, displacement on cracks comprising the damage produce a dynamic reduction in elastic moduli which results in the reduction of stored elastic potential energy available for rupture propagation. Second, off-fault energy dissipation due to frictional sliding and rapid opening of the micro-cracks also reduces energy available for propagation.

The effect of load on peak rupture velocity is summarized in Fig. 10. Increasing the applied load exacerbates the negative effect of damage on rupture in the '$T-$' direction which overwhelms the positive effect of an increased shear stress on the fault. Propagation in the '$C+$' direction is nearly the same for damaged and undamaged Homalite which supports our hypothesis that compression in the 'C' direction suppresses motion on the damage cracks.

References

Andrews, D.J., 1976. Rupture velocity of plane strain shear cracks. J. Geophys. Res. 81 (B32), 5679–5689.

Andrews, D.J., 2005. Rupture dynamics with energy loss outside the slip zone. J. Geophys. Res 110, 1307.

Andrews, D.J., Ben-Zion, Y., 1997. Wrinkle-like slip pulse on a fault between different materials. J. Geophys. Res. 102, 553–571.

Ben-Zion, Y., 2001. Dynamic ruptures in recent models of earthquake faults. J. Mech. Phys. Solids 49, 2209–2244.

Ben-Zion, Y., Sammis, C.G., 2003. Characterization of fault zones. Pure Appl. Geophys. 160 (3), 677–715.

Bhat, H.S., Biegel, R.L., Rosakis, A.J., Sammis, C.G. 2010. The Effect of Asymmetric Damage on Dynamic Shear Rupture Propagation II: With Mismatch in Bulk Elasticity. Tectonophysics 493, 263–271 (this issue).

Biegel, R.L., Sammis, C.G., 2004. Relating fault mechanics to fault zone structure. Adv. Geophys. 47, 65–111.

Biegel, R.L., Sammis, C.G., Rosakis, A.J., 2008. An experimental study of the effect of off-fault damage on the velocity of a slip pulse. J. Geophys. Res. 113 (B4).

Bizzarri, A., 2009. What does control earthquake ruptures and dynamic faulting? A review of different competing mechanisms. Pure Appl. Geophys. 166 (5), 741–776.

Bouchon, M., Bouin, M.P., Karabulut, H., Toksoz, M.N., Dietrich, M., Rosakis, A.J., 2001. How fast is rupture during an earthquake? New insights from the 1999 Turkey earthquakes. Geophys. Res. Lett. 28, 2723–2726.

Burridge, R., 1973. Admissible speeds for plane-strain self-similar shear cracks with friction but lacking cohesion. Geophys. J. Roy. Astron. Soc. 35, 439–455.

Cochard, A., Rice, J.R., 2000. Fault rupture bbetween dissimilar materials- Ill-posedness, regularization, and slip–pulse response. J. Geophy. Res. 105 (B11).

Harris, R.A., Day, S.M., 1997. Effects of a low-velocity zone on a dynamic rupture. B. Seismol. Soc. Am. 87 (5), 1267–1280.

Harris, R.A., Day, S.M., 2005. Material contrast does not predict earthquake rupture propagation direction. Geophys. Res. Lett. 32 (23), L23301, doi: 10.1029/2005GL023941.

Heaton, T.H., 1990. Evidence for and implications of self-healing pulses of slip in earthquake rupture. Phys. Earth Planet. Int. 64 (1), 1–20.

Li, Y.G., Malin, P.E., 2008. San Andreas Fault damage at SAFOD viewed with fault-guided waves. Geophys. Res. Lett. 35 (8).

Li, Y.G., Vidale, J.E., 2001. Healing of the shallow fault zone from 1994–1998 after the 1992 M 7. 5 Landers, California, earthquake. Geophys. Res. Lett. 28 (15), 2999–3002.

Li, Y.G., Vidale, J.E., Day, S.M., Oglesby, D.D., Cochran, E., 2003. Postseismic fault healing on the rupture zone of the 1999 M 7.1 Hector Mine, California, earthquake. B. Seismol. Soc. Am. 93 (2), 854–869.

Lu, X., Lapusta, N., Rosakis, A.J., 2007. Pulse-like and crack-like ruptures in experiments mimicking crustal earthquakes. P. Natl. Acad. Sci. USA 104 (48), 18,931–18,936, doi: 10.1073/pnas.0704268104.

Lu, X., Lapusta, N., Rosakis, A.J., 2008. Analysis of supershear transition regimes in rupture experiments: the effect of nucleation conditions and friction parameters. Subm. J. Geophys. Res.

Marone, C., Vidale, J.E., Ellsworth, W.L., 1995. Fault healing inferred from time dependent variations in source properties of repeating earthquakes. Geophys. Res. Lett. 22 (22), 3095–3098.

O'Connell, R.J., Budiansky, B., 1974. Seismic velocities in dry and saturated cracked solids. J. Geophys. Res 79 (35), 5412–5426.

Ranjith, K., Rice, J.R., 2001. Slip dynamics at an interface between dissimilar materials. J. Mech. Phys. Solids 49, 341–361.

Rice, J.R., 2001. In: Aref, H., Phillips, J.W. (Eds.), New Perspectives on Crack and Fault Dynamics, Mechanics for a New Millennium. Kluwer Academic Publishers, pp. 1–23.

Rice, J.R., Sammis, C.G., Parsons, R., 2005. Off-fault secondary failure induced by a dynamic slip pulse. Bull. Seismol. Soc. Amer. 95 (1), 109–134.

Rosakis, A.J., Xia, K.W., Lykotrafitis, G., Kanamori, H., 2007. Dynamic shear rupture in frictional interfaces: speeds, directionality and modes. In: Kanamori, H. (Ed.), Treatise in Geophysics, 4, pp. 153–192.

Rubin, A.M., Ampuero, J.P., 2007. Aftershock asymmetry on a bimaterial interface. J. Geophys. Res. 112, B05307, doi: 10.1029/2006JB004337.

Shi, Z.Q., Ben-Zion, Y., 2006. Dynamic rupture on a bimaterial interface governed by slip-weakening friction. Geophys. J. Int. 165, 469–484.

Templeton, E.L., Rice, J.R., 2007. Off-fault plasticity and earthquake rupture dynamics, 1. Dry materials or neglect of fluid pressure changes. J. Geophys. Res. (subm.).

Weertman, J., 1980. Unstable slippage across a fault that separates elastic media of different elastic constants. J. Geophys. Res 85 (83), 1455–1461.

Xia, K.W., Rosakis, A.J., Kanamori, H., 2004. Laboratory earthquakes: the sub-Rayleigh-to-supershear rupture transition. Science 303, 1859–1861.

Xia, K.W., Rosakis, A.J., Kanamori, H., 2005a. Supershear and sub-Rayleigh to supershear transition observed in laboratory earthquake experiments. Exp. Tech. 29, 63–66.

Xia, K.W., Rosakis, A.J., Kanamori, H., Rice, J.R., 2005b. Laboratory earthquakes along inhomogeneous faults: directionality and supershear. Science 308, 681–684.